Evaluation of Orientation Ambiguity and Detection Rate in April Tag and WhyCode

Joshua Springer
Department of Computer Science
Reykjavík University
Reykjavík, Iceland
joshua19@ru.is

Marcel Kyas
Department of Computer Science
Reykjavík University
Reykjavík, Iceland
marcel@ru.is

Abstract—Fiducial systems provide a computationally cheap way for mobile robots to estimate the pose of objects, or their own pose, using just a monocular camera. However, the orientation component of the pose of fiducial markers is unreliable, which can have destructive effects in autonomous drone landing on landing pads marked with fiducial markers. This paper evaluates the April Tag and WhyCode fiducial systems in terms of orientation ambiguity and detection rate on embedded hardware. We test 2 April Tag variants – 1 default and 1 custom – and 3 Whycode variants – 1 default and 2 custom. We determine that they are suitable for autonomous drone landing applications in terms of detection rate, but may generate erroneous control signals as a result of orientation ambiguity in the pose estimates.

Index Terms—fiducial, marker, orientation, ambiguity, pose

I. INTRODUCTION

Fiducial markers provide a computationally cheap way to estimate the pose (position + orientation) of objects, or for a robot to estimate its own pose in an environment. Given a monocular image and the distortion parameters of the camera that produced it, a fiducial system can quickly determine if the image contains one of its markers, and can determine the marker's pose. While the position component of the pose is typically accurate, the orientation is often subject to ambiguity (see Section III), such that it (and the pose to which it belongs) has discontinuities when viewed as a time series. One way of evaluating the ability of a fiducial system to accurately determine the orientation of the marker, without having a sophisticated system to know the marker's ground-truth pose, is to detect discontinuous poses perceived from fiducial markers attached to physical objects. Further, since mobile robots that can benefit from fiducial markers use embedded hardware with limited computational capacity, it is useful to know the rate at which the fiducial system can detect markers when executing on such hardware. Previous work tends to use a downward-facing camera that is fixed on the drone or stabilized on a gimbal, but does not actuate in order to track the landing pad; our evaluation informs subsequent autonomous drone landing tests, where a drone actuates its camera in order to actively track a landing pad that is marked with a fiducial marker [1]. The drone uses the marker's pose to generate position targets in order to approach and land on the landing pad. In this scenario, pose discontinuities caused by orientation ambiguity propagate to the drone's control signals

(a) April Tag 48h12   (b) WhyCode

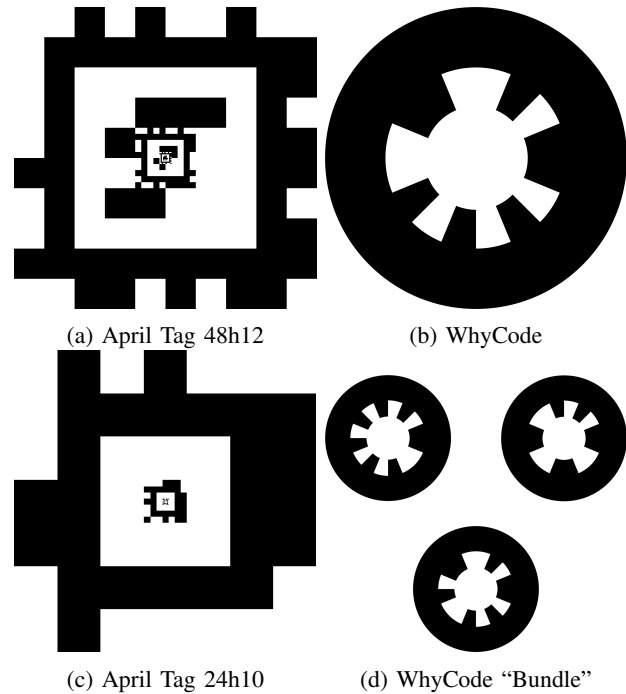(c) April Tag 24h10   (d) WhyCode "Bundle"

Fig. 1: The fiducial markers evaluated in this paper.

and cause erratic behavior. Moreover, in such a time-sensitive scenario, the pose estimation must be fast, motivating our evaluation of the systems' detection rates.

We evaluate a total of 5 fiducial systems, 2 of which are the default, unmodified systems of April Tag 48h12 and WhyCode (Figures 1a and 1b respectively). We also tested three modified versions of the default systems: 1) our "WhyCode Ellipse" variant which uses the same marker as in Figure 1b but uses additional image sampling points to inform its decision of the marker's orientation, 2) our "WhyCode Multi" variant, which uses the marker arrangement in Figure 1d to determine the orientation of the plane connecting the markers, and then assigns that orientation to all of the markers, and 3) the April Tag 24h10 variant, a smaller version of April Tag 48h12. We focus on monocular fiducial systems because they are computationally cheap and can therefore execute on embedded hardware onboard a drone, and they are cheap to deploy,

requiring only a printout of a particular marker, and a monocular camera (arguably the most common drone peripheral sensor), There are many possible fiducial systems [2]–[6], but we choose those that are highly configurable, open source, and whose positional accuracy has been formally evaluated. Some systems that address the issue of orientation ambiguity (such as Lentimark [7] and the filtering method described in [8]) involve fundamental changes to the marker systems or are proprietary and are, therefore, less widely used. We aim to produce simpler solutions requiring minimal changes to existing marker systems to allow easy integration.

II. BACKGROUND

Fiducial markers are 2-dimensional patterns whose positions (and IDs) can accurately be determined in space using only images, without a notion of time. WhyCode [4] (shown in Figure 1b and 1d) is a lightweight, circular fiducial marker system, formed by an inner white circle, outer black circle, and a Manchester encoded ID between the two circles. April Tag [6], [9], [10] (shown in Figures 1a and 1c) is a square marker system with a configurable layout white and black squares, each representing a data bit or a section of the black and white border.

It is difficult to determine the orientation of planar fiducial markers using single-image, monocular systems, due to the fact that a marker may have the same appearance when viewed from specific, different angles. This orientation ambiguity typically results in apparent discontinuities in a marker's orientation when it is viewed as a time series. If the full marker pose (position + orientation) is used as a control input to the drone, these discontinuities can cause potentially destructive, erratic behavior. Therefore, it is easier to achieve stable precision drone landing using a fixed, downward-facing camera, so that the control algorithm needs only to consider the position of the fiducial marker and can ignore its orientation. Conversely, a marker system that avoids these discontinuities would enable gimbal-based marker tracking and therefore more reliable precision landing.

III. RELATED WORK

Irmisch [11] has analyzed the performance of April Tag and WhyCon markers in terms of their abilities to determine correct position in real world experiments. The experiments show that both April Tag and WhyCon have relatively low position estimate errors. The issue of ambiguity in planar marker orientation is a known problem, and various methods exist which attempt to mitigate it. One example is an edition of ARTag called LentiMark [7], which uses special Moiré patterns on the outside of the tags to determine a correct orientation. Another study [8] proposes to determine the correct solution using an averaging algorithm with multiple views of the markers, instead of using only a single image. The method in [12] proposes to consider the marker as a moving object, and therefore reduces orientation ambiguity by intelligently choosing the orientation using a motion model.

IV. METHODS

We captured the video stream at 480p with a "Creative Technology Live! Cam Sync 1080p." The camera has a wide angle of 77 degrees. We mounted the markers to a divider wall and moved the camera by hand to simulate the drone's approach, and tested at distances of 1 to 3 meters, as relevant in the subsequent autonomous drone landing scenario [**?**]. We performed the experiments in a lab room at Reykjavik University, allowing us to control the light, whereas outdoor environments have variable light conditions and spectral signatures [13]. We use the position targets to evaluate the systems' performance in terms of the reliability of the control signals they would send to a drone (orientation ambiguity), and at what frequency the system recognizes the landing pad at all (detection rate).

A. ROS Message Attributes and Calculations

April Tag and WhyCode both have ROS (Robot Operating System) [14] modules that allow them to interact with other programs, such as flight control software. We have extended them to perform calculations and include message attributes for drone landing:

1) A **position target** in the a relative "east, north, up" (ENU) coordinate frame *whose origin is the camera*, where "east" refers to the camera's right, "north" to the front, and "up" to the top. This parameter gives the relative position from the camera to the marker, under the assumption that the marker is flat on the ground, facing up. In an autonomous drone landing scenario, this parameter tells the drone where to go in order to approach the marker.

2) The **normalized pixel position** $u_n, v_n \in [-1, 1]$ of the center of each marker, which serves as inputs to the systems that track the marker.

3) The marker's **orientation components**: yaw, pitch, and roll. Our edits exposed these to the ROS interfaces in the cases where they were not explicitly exposed. An autonomous drone can use the marker's yaw to align itself to the landing pad before descent.

B. Tested Fiducial Systems

1) WhyCode Orig: We use a version of WhyCode created by Ulrich [15] as a baseline for testing. The method samples the ellipse that goes through the centers of the "teeth" forming the marker's ID (i.e. the yellow and green ellipses in Figure 4), to determine the marker's orientation. Of the two possible candidate solutions that are implied by the detected semi-axes of the outer black ellipse, the detector chooses the one with a lower variance in the number of sample points per tooth. This works because the candidate solutions predict this ellipse to be in slightly different places, and the correct solution should predict the ellipse to be in its correct place, minimizing the variance in the number of sample points that coincide with each tooth. Conversely, the incorrect solution should predict the ellipse to be in the incorrect place, such that the sampling ellipse does not line up well with the marker, and the variance

Fig. 2: An illustration of the method in [15] that determines an orientation of the marker based on which ellipse is better centered on the marker. It chooses the ellipse that minimizes the variances in the ellipse's intersection with the teeth. Both possible solutions are shown, with the green being correct.
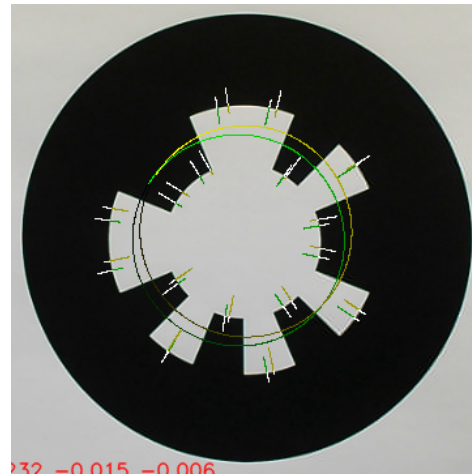

Fig. 3: An illustration of "WhyCode Ellipse". Each ellipse and corresponding radial lines represent the sampling locations, marked in yellow and green to distinguish the two candidate solutions. This method uses the radial lines to determine how well each candidate solution is aligned with the real image. In this case, the green solution is correct and is visually better centered on the marker.

is higher. We use WhyCode markers with 8-bit IDs so that there are several sample points and a meaningful variance.

2) WhyCode Ellipse: The first method that we have implemented for reducing orientation ambiguity is the `ellipse_sampling` branch of [16]. The method determines the marker ID and the two candidate solutions for the orientation as in WhyCode Orig, after which it identifies the lines that go from the center of the white region through the center of each tooth. It then samples the input image on these lines, as illustrated by Figure 4. It expects a white-to-black transition at the predicted edge of each tooth, and the sampling line is centered on this edge. The true edge is determined during sampling, and its value is recorded as a percentage of the length of the line segment, oriented such that 0 corresponds to the centermost end of the line segment, and 1 corresponds to its outermost end. The detector chooses the solution that minimizes the variance of the location of the true edge over the sample lines.

3) WhyCode Multi: The second method that we have implemented for reducing orientation ambiguity (the `multi` branch of [16]) works under the assumption that all recognized markers are coplanar. For each input image, the WhyCode algorithm identifies all markers and then finds the normal vector to the plane implied by the markers' positions, after which it can calculate the pitch and roll components of the bundle's orientation. The position of the bundle is the mean of the positions of its constituent markers, and its yaw is that of any constituent markers, with the assumption they are all the same. The detector then calculates all additional attributes for the bundle as if it were a single marker. This system uses the arrangement of WhyCode markers in Figure 1d.

4) April Tag 48h12: April Tag provides a default family 48h12, shown in Figure 1a, for which the 4 center squares are undefined, 20 squares provide a white border, 28 squares
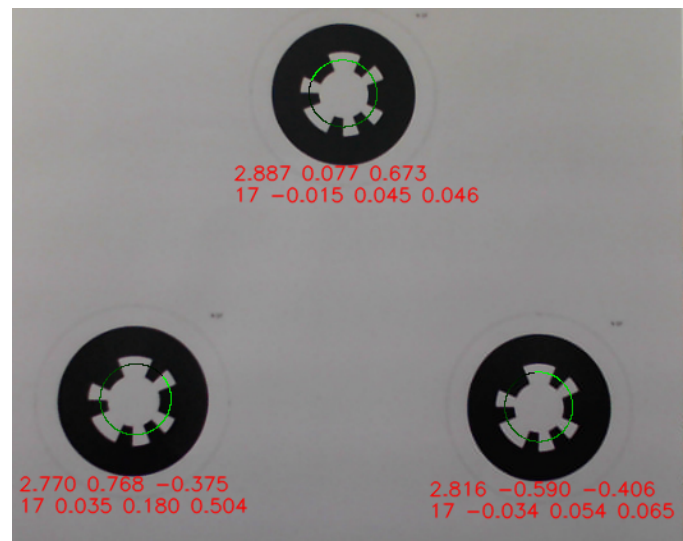

Fig. 4: An illustration of "WhyCode Multi". The system regresses a plane connecting the markers, then assigns that orientation to each marker, as they are assumed to be coplanar.

provide a black border, and 48 squares provide data bits, giving a total of 96 defined squares. The undefined center provides a space to embed a smaller marker, which is useful in the last stages of a drone landing scenario, where the camera is too close to the landing pad to see the larger markers. We test this family as a baseline for the performance of April Tag.

5) April Tag 24h10: April Tag provides libraries to specify and generate non-default marker variants, from which we generated the April Tag 24h10 family (shown in Figure 1c). This variant maintains marker embeddability while decreasing

the size of the marker definition, by reducing the size of the undefined center to one square, and adjusting the surrounding regions accordingly: Eight squares for a white border, 16 squares for a black border, and 24 outer data squares. This gives a total of 48 defined squares(compared to the 96 squares of April Tag 48h12). This reduction is important because all possible valid marker IDs for each family are loaded into a single hash table at runtime, and April Tag 48h12 has a large hash table of 42,211 markers which can require more than 1 GB of RAM – a precious resource on embedded hardware. By contrast, April Tag 24h10 has only 18 markers and therefore requires significantly less memory. We test April Tag 24h10 to see if it can offer an increase in detection rate with respect to April Tag 48h12.

C. Bases of Comparison

1) Discontinuities: Orientation ambiguity manifests as discontinuities (e.g. sign flips and other spikes) in the pitch and roll components of a marker's orientation, which propagate to subsequent calculations that depend on the orientation – *the position targets*. The fiducial systems are compared on the basis of the number of discontinuities in the position targets they generate. A "good" system minimizes this number.

We capture 33 videos of the marker arrangement in Figure 1, printed, so each marker has a side length of 30 cm, and mounted to a planar surface with clear lighting. We move the camera in each of the videos (e.g. panning, tilting, moving in and out, etc.) while keeping all markers completely in the frame at all times. We save the videos as a series of pairs of image and camera info messages in the standard ROS way, using `rosbag`. Each fiducial system in Section IV-B processes the same set of videos. Since the experiments are conducted slowly in a controlled environment, angular and linear speeds above pre-determined thresholds can be classified as discontinuities. Linear discontinuities occur when the quotient of any position target $\vec{P} = \langle p_e, p_n, p_u \rangle$ (east, north, or up) and its predecessor is sufficiently negative (such discontinuities always occur over the origin):

$$\frac{p_{x,i+1}}{p_{x,i}} < \theta_l < 0 \tag{1}$$

where $p_{x,i}$ and $p_{x,i+1}$ are position targets in a single dimension $x \in \{e, n, u\}$ dimension at frames i and $i+1$ respectively, and $\theta_l < 0$ is an experimentally determined threshold (see Table I). If the inequality in Equation 1 is true, this implies that the marker appears to change locations faster than allowed during testing.

Similarly, a discontinuity determined from angular speed s_a occurs when

$$s_a = \frac{\text{dist}(q_i, q_{i+1})}{\Delta t} > \theta_a > 0 \tag{2}$$

where q_i and q_{i+1} are the quaternions representing the orientation of a marker at frames i and $i+1$, respectively, $\text{dist} \geq 0$ is the intrinsic geodesic distance between the angles represented by the quaternions, Δt is the change in time between frames i and $i+1$, and θ_a is a pre-determined threshold (see Table I).

If the inequality in Equation 2 is true, this implies that the marker appears to rotate faster than allowed during testing.

We consider cases where Equations 1 and 2 are true simultaneously, to reduce false identification of discontinuities. For example, a linear discontinuity can appear erroneously via noise when the e or n component of a marker's position target is close to 0. If both discontinuities occur at the same time, this means that the marker truly appears to drastically change positions in space in a small amount of time, which does not happen in our test cases. Finally, since the test cases vary in length, we can define a "discontinuity rate" $r_d = \frac{d}{n}$ which describes the number of discontinuities d as a portion of the total number of detections n, and which serves as a basis for comparing the performance of each system in each test case.

2) Detection Rate: We capture 14 videos of each marker in Figure 1 separately with both the camera and marker remaining still, at several distances and deflections from one another. We record videos of each marker in isolation to avoid any potential interference, since the marker detectors all analyze black and white regions. Both the camera and marker remain still during each test case, and each test case lasts 60 s. The systems are compared on the basis of their detection rate (Hz) when executing on a Raspberry Pi 4 with 2 GB of RAM, with the following ROS pipeline: replaying a test case video, image rectification using `image_proc` (April Tag systems only, required by April Tag ROS module), marker detection by each of the fiducial systems in Section IV-B, and rosbag recording for later analysis. This avoids capturing the image during testing, but maintains fairness of comparison among the systems, since all systems are put into the same computational environment one at a time, and all process similar test cases. We then determine a detection rate $F = \frac{n}{t}$, where n is the number of detections, and t is the length in seconds of the test case. The goal of this metric is to determine at what frequency the embedded hardware can run the fiducial system. All systems process video from the same camera at the same framerate, so the setup is not biased in favor of any particular system.

We use the default system parameters for both April Tag and WhyCode. We also test only with the markers in Figure 1, as these are the markers that we use to mark landing pads.

V. RESULTS

Figures 5 and 6 give an intuition for the discontinuities studied in this paper. Figure 5 shows the east, north, and up position targets for a test case where the camera moves first to the left, then to the right, keeping the marker near the center of the frame the entire time – "orbiting" the marker. The east position target correctly indicates the camera's movement left and right, while the north and up position targets correctly remain near-constant (the camera was being moved by hand, so there is some erroneous movement). Figure 6 shows the next test case with the same marker and same camera movement, but from a longer distance (indicated by the lower up position target). Since the marker is farther away and therefore smaller in the camera frame, it is more difficult for the system to
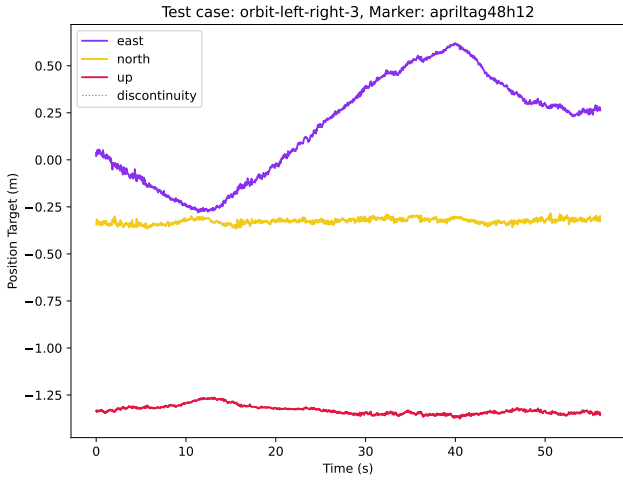
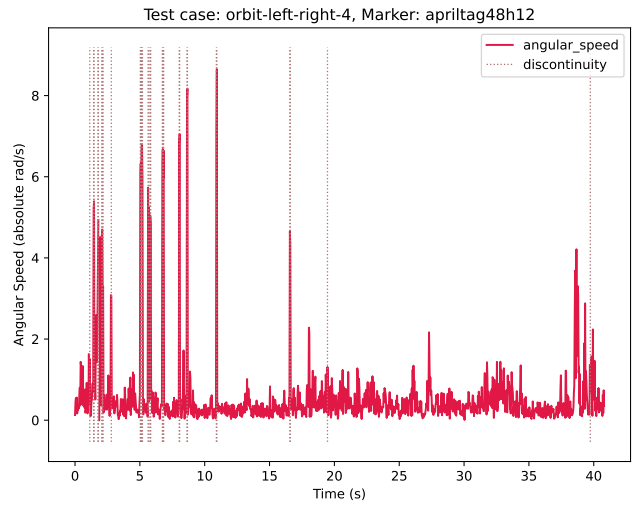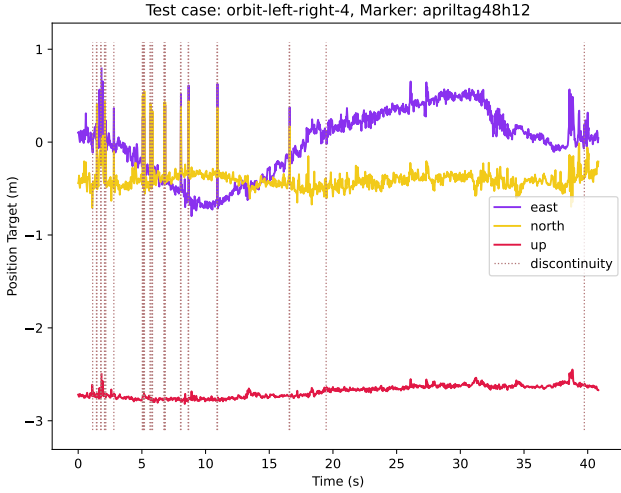Fig. 5: Example of position targets without discontinuities.

Fig. 6: Example of discontinuities in position targets (marked by the vertical lines), which are spikes in the east and north position targets that roughly correspond to sign flips.

estimate its orientation, leading to the discontinuities. The discontinuities always occur over the origin – the camera appears to jump from one side of the marker to the other. Notice the spikes in the east position target $t \in [25, 30]$s in Figure 6 are not discontinuities, but rather noise. Further, noise in the east position target in both Figures 5 and 6 would be considered discontinuities when the position target becomes near-zero, such that noisy movement actually satisfies Equation 1. Figure 7 shows the detected angular speed of the marker in Figure 7, showing that certain spikes in Figure 6 are not considered discontinuities because they do not correspond in time to spikes in angular speed. Figure 8 visualizes the discontinuity rates for the systems, and Figure 9 visualizes their detection rates. Table I shows the speed thresholds for Equations 1 and 2.

Fig. 7: The angular speeds of the marker in Figure 6, similarly labeled with discontinuities.

Discontinuity Type	Symbol	Value
rotational	θ_a	1.0 rad/s
linear	θ_l	-0.8 (unitless)

TABLE I: Thresholds for targeting pose discontinuities in all systems. We say that a discontinuity occurs when the inequalities in Equations 1 and 2 are simultaneously true using the values in this table. These are chosen to be well above the maximum allowed values in testing, so that they are not sensitive to noise.
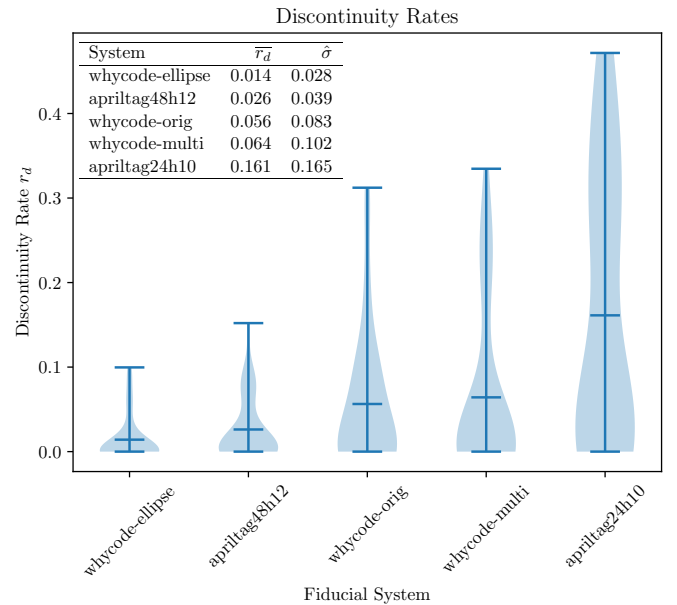

System	$\overline{r_d}$	$\hat{\sigma}$
whycode-ellipse	0.014	0.028
apriltag48h12	0.026	0.039
whycode-orig	0.056	0.083
whycode-multi	0.064	0.102
apriltag24h10	0.161	0.165

Fig. 8: A visualization of the discontinuity rates r_d, which represent the proportion of discontinuous position target readings relative to the total number of readings. $\overline{r_d}$ is the sample mean of the discontinuity rate, and $\hat{\sigma}$ is the sample standard deviation, and $n = 33$ per group.
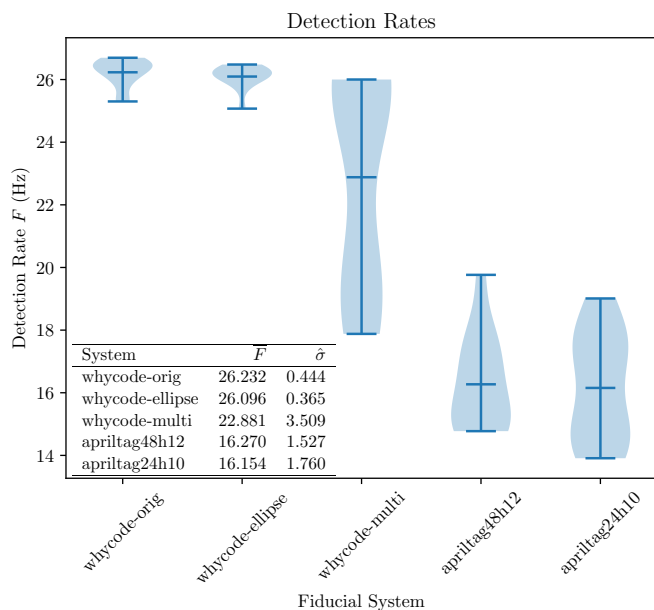
Fig. 9: A visualization of the detection rates F (Hz). $\overline{F}$ is the sample mean of the detection rate, and $\hat{\sigma}$ is the sample standard deviation, and $n = 14$ per group.

System	$\overline{F}$	$\hat{\sigma}$
whycode-orig	26.232	0.444
whycode-ellipse	26.096	0.365
whycode-multi	22.881	3.509
apriltag48h12	16.270	1.527
apriltag24h10	16.154	1.760

VI. DISCUSSION

WhyCode Ellipse offers a decrease in discontinuity rate compared to WhyCode Orig, with only a small decrease in detection rate. WhyCode Multi does not offer a decrease in discontinuity rate compared to WhyCode Orig, and also has a lower detection rate. It is possible that variations in the orientation of the plane connecting WhyCode Multi markers could be reduced by adding more markers to the arrangement, or spreading them out. April Tag 24h10 has a higher discontinuity rate than April Tag 48h12, with no increase in detection rate. The lower detection rates of the April Tag systems are likely a result of their longer ROS pipeline, which depends on transmitting each input image to an intermediate `image_proc` node and back for rectification. WhyCode builds this into its algorithm, thereby avoiding latency and performing faster than April Tag even when detecting several markers at a time. However, WhyCode systems cannot handle marker embedding as April Tag systems can.

We use only the default system parameters, and a single hardware setup. Different setups will have different results, e.g. a camera with a telephoto lens might provide more accuracy at long distances, but would require calibration at many different focal lengths. Different computational hardware will also give different detection rates.

VII. CONCLUSION & FUTURE WORK

We have evaluated 5 fiducial systems - 2 existing variants: April Tag 48h12 and WhyCode Orig, and 3 custom variants which we have implemented - in terms of their rates of discontinuity in position target generation and detection rate on a Raspberry Pi 4 (2 GB RAM). We have determined

that WhyCode Ellipse, WhyCode Multi, April Tag 48h12, and WhyCode Orig provide a good starting point for testing gimbal-based fiducial landing with a drone, while April Tag 24h10 is likely to exhibit problematic behavior. These markers are further evaluated in our subsequent study [1].

Future tests of the WhyCode Multi system could use different marker arrangements, such as with more markers, or with the markers spaced farther apart. All systems could be further tested with different runtime parameters, cameras, computational hardware, and lighting conditions.

REFERENCES

[1] J. Springer and M. Kyas, "Autonomous Drone Landing with Fiducial Markers and a Gimbal-Mounted Camera for Active Tracking," in *2022 IEEE International Conference on Robotic Computing*, 2022.

[2] M. Fiala and M. Fiala, "ARTag, a fiducial marker system using digital techniques," in *Proceedings of the 2005 IEEE Computer Society Conference on Computer Vision and Pattern Recognition (CVPR'05) - Volume 2 - Volume 02*, ser. CVPR '05. Washington, DC, USA: IEEE Computer Society, 2005, pp. 590–596.

[3] S. Garrido-Jurado, R. Muñoz-Salinas, F. Madrid-Cuevas, and M. Marín-Jiménez, "Automatic generation and detection of highly reliable fiducial markers under occlusion," *Pattern Recognition*, vol. 47, p. 2280–2292, 06 2014.

[4] P. Lightbody, T. Krajník, and M. Hanheide, "A Versatile High-performance Visual Fiducial Marker Detection System with Scalable Identity Encoding," in *Proceedings of the Symposium on Applied Computing*, ser. SAC '17. New York, NY, USA: ACM, 2017, pp. 276–282.

[5] M. Nitsche, T. Krajník, P. Čížek, M. Mejail, and T. Duckett, "Whycon: An efficent, marker-based localization system," in *IROS Workshop on Open Source Aerial Robotics*, 2015. [Online]. Available: https://core.ac.uk/download/pdf/42583963.pdf

[6] E. Olson, "AprilTag: A Robust and Flexible Visual Fiducial System," in *2011 IEEE International Conference on Robotics and Automation*, 2011, pp. 3400–3407.

[7] H. Tanaka, Y. Sumi, and Y. Matsumoto, "A solution to pose ambiguity of visual markers using Moiré patterns," in *2014 IEEE/RSJ International Conference on Intelligent Robots and Systems*, 2014, pp. 3129–3134.

[8] S.-F. Ch'ng, N. Sogi, P. Purkait, T.-J. Chin, and K. Fukui, "Resolving Marker Pose Ambiguity by Robust Rotation Averaging with Clique Constraints," 2019.

[9] J. Wang and E. Olson, "Apriltag 2: Efficient and robust fiducial detection," 10 2016, pp. 4193–4198.

[10] M. Krogius, A. Haggenmiller, and E. Olson, "Flexible layouts for fiducial tags," in *2019 IEEE/RSJ International Conference on Intelligent Robots and Systems (IROS)*, 2019, pp. 1898–1903.

[11] P. Irmisch, "Camera-based Distance Estimation for Autonomous Vehicles," 12 2017.

[12] P.-C. Wu, Y.-H. Tsai, and S.-Y. Chien, "Stable pose tracking from a planar target with an analytical motion model in real-time applications," 11 2014.

[13] J. Hedgecoe, *John Hedgecoe: The New Manual of Photography*. DK Pub., 2003.

[14] M. Quigley, K. Conley, B. Gerkey, J. Faust, T. Foote, J. Leibs, R. Wheeler, and A. Ng, "ROS: an open-source Robot Operating System," vol. 3, 01 2009.

[15] J. Ulrich, "Fiducial Marker Detection for Vision-based Mobile Robot Localisation," pp. 18–21, 2020, Bachelor Thesis.

[16] Joshua Springer. (2020) Edited WhyCon/WhyCode Repository. "https://github.com/uzgit/whycon-ros". (accessed: 2022.2.2). [Online]. Available: https://github.com/uzgit/whycon-ros